

Evolution of Constitution, Structure, and Morphology in FeCo-Based Multicomponent Alloys

R. LI, M. STOICA, G. LIU, and J. ECKERT

Constituent phases, melting behaviors, and microstructure of multicomponent $(\text{Fe}_{0.5}\text{Co}_{0.5})_x\text{-(Mo}_{0.1}\text{C}_{0.2}\text{B}_{0.5}\text{Si}_{0.2})_{100-x}$ alloys ($x = 95, 90, 85, 80,$ and 70) produced by copper mold casting were evaluated by various analysis techniques, *i.e.*, X-ray diffractometry, scanning electronic microscopy with energy dispersive X-ray spectrometry, and differential scanning calorimetry. Metastable Fe_3C - and Cr_{23}C_6 -type phases were identified in the chill-cast alloys. A schematic illustration was proposed to explain the evolution of constituent phases and microstructure for the alloys with $x = 95, 90,$ and 85 during the solidification process, which could be applicable to controlling microstructural formation of other multicomponent alloys with similar microstructures by artificially adjusting the composition.

DOI: 10.1007/s11661-009-0052-6

© The Minerals, Metals & Materials Society and ASM International 2009

I. INTRODUCTION

IT is well known that bulk metallic glasses (BMGs) are a family of advanced ultrahigh strength materials, which have been investigated intensively.^[1–3] However, the intrinsic brittleness and strict fabrication conditions of these BMGs limit their further application as advanced structural materials.^[4] Recently, dendrite-eutectic (D-E) composites were developed in Ti-, Fe-, Cu-, Mg-, and Al-based chill-cast multicomponent hypoeutectic alloys as a competitive replacement of BMGs.^[5–12] Compared to the BMGs with close chemical compositions, this kind of D-E composite shows similar strength and remarkable plasticity as well as a more controllable production process. Normally, the microstructure of the hypoeutectic alloys is characteristic of soft dendrite (a terminal solid solution phase of basis element) embedded into hard eutectics (a networklike framework phase). Many reports indicate that the outstanding mechanical properties can be related to the composite structure of soft and hard phases with appropriate morphology and deformation behavior.^[5,6,8,9,13] Since most of the valuable information for hypoeutectic alloys is focused in binary, ternary, and a few conventional multicomponent systems, the investigation of phase constituent and microstructural evolution dependent on chemical composition in multicomponent alloys may reveal information about

controlling the morphological structure and optimizing the mechanical properties of this kind of D-E composite.

Most recently, we produced a family of FeCo-based D-E composites with high strength and large plasticity through adding eutectic-forming elements (*i.e.*, Mo, C, B, and Si) with fixed atomic ratios into equiatomic FeCo alloy by copper mold casting.^[13] Compared to the brittle binary precursor alloy, these chill-cast FeCo-based multicomponent alloys exhibit remarkable improvement of yield strength and plastic deformation. In this article, we evaluated the effect of composition adjustment on thermal properties, phase constituent, and morphological characteristics of $(\text{Fe}_{0.5}\text{Co}_{0.5})_x\text{-(Mo}_{0.1}\text{C}_{0.2}\text{B}_{0.5}\text{Si}_{0.2})_{100-x}$ ($x = 95, 90, 85, 80,$ and 70) alloys. The forming condition and morphology of metastable phases in our alloys will be discussed. A possible evolution of constituent phases and microstructure for the $x = 95, 90,$ and 85 alloys during the solidification process was illustrated, which can be beneficial to understanding the morphologic formation of these D-E composites.

II. EXPERIMENTAL PROCEDURE

Mixtures of pure Fe, Co, Mo, Si, B, and C with purity above 99.9 mass pct at least were used to produce 100 to 200 g prealloys with nominal atomic composition of $(\text{Fe}_{0.5}\text{Co}_{0.5})_x\text{-(Mo}_{0.1}\text{C}_{0.2}\text{B}_{0.5}\text{Si}_{0.2})_{100-x}$ ($x = 95, 90, 85, 80,$ and 70) using an induction furnace in a high-purity argon atmosphere. Pieces of the prealloys were remelted in quartz tubes and then injected into a water-cooled copper mold in a high-purity argon atmosphere to produce chill-cast rods with a dimension of $\phi 3 \times 50$ mm. The phase structure was examined using a Philips X'Pert PW 3040 diffractometer (Philips Analytical X-ray B.V., Almelo, The Netherlands) with $\text{Co } K_\alpha$ radiation at a scanning rate of 0.6 deg/min. The lattice parameter of $\alpha\text{-(Fe,Co)}$ phase was identified using the same XRD equipment at a slower scanning rate of

R. LI, Guest Scientist, M. STOICA, Research Staff Member, and G. LIU, Guest Scientist, are with the Institute for Complex Materials, IFW Dresden, D-01171 Dresden, Germany. Contact e-mail: m.stoica@ifw-dresden.de J. ECKERT, Professor, is with the Institute for Complex Materials, IFW Dresden, and the Institute of Materials Science, TU Dresden, D-01062 Dresden, Germany.

This article is based on a presentation given in the symposium "Bulk Metallic Glasses VI," which occurred during the TMS Annual Meeting, February 15–19, 2009, in San Francisco, CA, under the auspices of TMS, the TMS Structural Materials Division, TMS/ASM: Mechanical Behavior of Materials Committee.

Article published online November 24, 2009

0.06 deg/min in the 2θ range of 98 to 104 deg. The melting behaviors of the as-cast samples were evaluated with a Netzsch DSC 404 C *Pegasus** differential

*Netzsch DSC 404 C *Pegasus* is a trademark of NETZSCH Gerätebau GmbH, Selb/Bayern, Germany.

scanning calorimeter (DSC) with a vacuum-tight construction at heating rates of 0.33 K/s under a flow of high-purity argon. The microstructure of these D-E composites was examined by scanning electronic microscopy (SEM) using a Gemini LEO 1530 microscope equipped with a Bruker energy-dispersive X-ray spectrometer (EDX).** The observed surface was etched

**Bruker EDX is a trademark of Bruker AXS Ltd., Coventry, UK.

in a 5 vol pct nitric acid–ethanol mixture for 10 to 25 seconds. The collection time of element mapping analysis using EDX is about 2 hours for the tested samples at 5 and 20 kV, respectively, to ensure enough signal collection from minor elements. Morphological characteristics of average linear sizes (l) and volume fractions (f) of constituent phases were measured by quantitative microscopy analysis.^[14] At least five continuous typical images in the same magnification for each sample were analyzed to ensure the reliability of the results.

III. RESULTS AND DISCUSSION

Figure 1 shows the XRD patterns of $(\text{Fe}_{0.5}\text{Co}_{0.5})_x(\text{Mo}_{0.1}\text{C}_{0.2}\text{B}_{0.5}\text{Si}_{0.2})_{100-x}$ ($x = 95, 90, 85, 80,$ and 70) as-cast rods. When the FeCo concentration (x) is in the range from 95 to 85, only two crystalline phases can be identified in these chill-cast FeCo-based multicomponent alloys. One is α -(Fe,Co) solid solution phase; the other is the metastable o -(Fe,Co)₃(B,C) phase. As x is further decreased, an additional complex metastable phase, $(\text{Fe,Co})_{23}(\text{B,C})_6$, can be found in the samples for $x = 80$ and 70 . The relative intensity of the diffraction peaks belonging to the α -(Fe,Co) phases decreases with reducing the FeCo content, indicating less volume fraction of the α -(Fe,Co) phases in the corresponding alloys. Furthermore, the lattice parameters (a) of α -(Fe,Co) phase identified through the slow scanning mode of XRD are listed in Table I. The value of a slowly decreases with reducing x in the multicomponent alloys. The results of element mapping (not shown here) indicate that Si is enriched in α -(Fe,Co) phase and Mo is enriched in o -(Fe,Co)₃(B,C). Because the atomic size of the Si solute atom is smaller than the one of the Fe/Co solvent atom, the formation of α -(Fe,Co,Si) substitution solid solution could be responsible for the decrease of a .^[15] Combining this with the results from EDX analysis, the ratio of Fe and Co contents is found to be near 1 : 1 in all crystalline phases, which indicates Fe and Co atoms equivalently participate in phase formation.

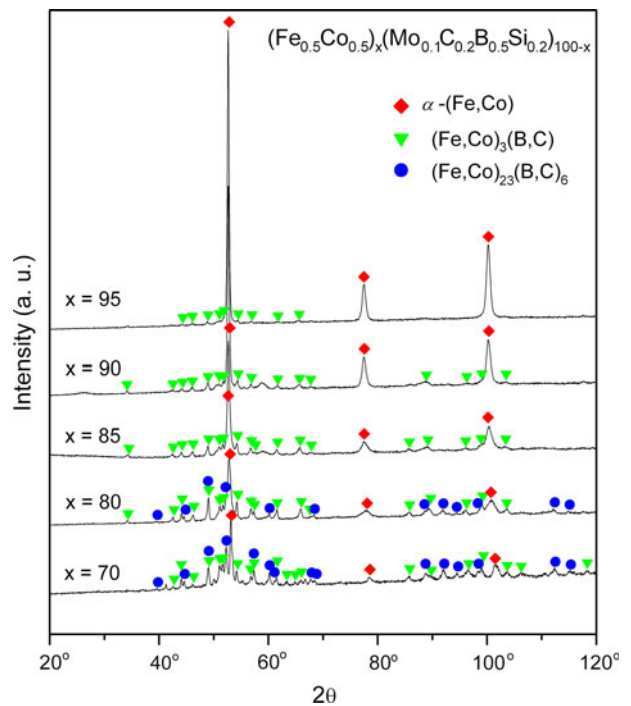


Fig. 1—XRD patterns of $(\text{Fe}_{0.5}\text{Co}_{0.5})_x(\text{Mo}_{0.1}\text{C}_{0.2}\text{B}_{0.5}\text{Si}_{0.2})_{100-x}$ alloys ($x = 95, 90, 85, 80,$ and 70).

Some results have been presented to describe the formation conditions of metastable Fe-(B,C) phases.^[16–20] Three types of Fe-B metastable compounds, t -Fe₃B (high-temperature tetragonal phase with a structure type of Ni₃P), o -Fe₃B (low-temperature orthorhombic phase with a structure type of Fe₃C), and Fe₂₃B₆ (a complex cubic phase with a structure type of Cr₂₃C₆), have been reported at the Fe-rich terminal in the binary Fe-B system produced by rapid solidification.^[16–18] Furthermore, in the Fe-C-B ternary system, the introduction of C could promote the stability of o -Fe₃(B,C) and Fe₂₃(B,C)₆ phases with the same structure types considering easier fabrication conditions.^[17,19] The lattice parameters show a linear dependence on the B/C content,^[20] which indicates that the atomic concentration of B/C in two compounds is changeable with the chemical composition of matrix phases. In our FeCo-based multicomponent alloys, the equilibrium Fe₂B-type phase disappears in all chill-cast samples, which is replaced with the nonequilibrium o -(Fe,Co)₃(B,C) and $(\text{Fe,Co})_{23}(\text{B,C})_6$ phases. The Cr₂₃C₆-type metastable phase can only be found in the FeCo-based alloys with x range from 80 to 70, *i.e.*, with an atomic ratio between (Fe,Co) and (B,C) near 4 : 1.

Figure 2 shows the melting behaviors of these FeCo-based chill-cast alloys. The melting temperature (T_m) and liquidus temperature (T_l) are summarized in Table I. For the samples with x from 95 to 85, the DSC curves show two obvious endothermic peaks during the melting process. One is near liquidus; the other is near solidus. With decreasing x , T_l of the corresponding samples reduces gradually, while T_m almost maintains a constant temperature, which indicates that these three

Table I. Parameters of Morphology and Physical Properties of $(\text{Fe}_{0.5}\text{Co}_{0.5})_x(\text{Mo}_{0.1}\text{C}_{0.2}\text{B}_{0.5}\text{Si}_{0.2})_{100-x}$ Alloy ($x = 100, 95, 90, 85, 80,$ and 70)*

Alloy	f_d (Pct)	l_d (mm)	l_e (μm)	a (\AA)	T_m (K)	T_l (K)	σ_y (MPa)	ε_y (Pct)	σ_c (MPa)	ε_p (Pct)	ρ (g/cm^3)
$(\text{Fe}_{0.5}\text{Co}_{0.5})_{95}(\text{Mo}_{0.1}\text{C}_{0.2}\text{B}_{0.5}\text{Si}_{0.2})_5$	79.8	6.1 ± 3.7	0.95 ± 0.83	2.8548	1362	1715	1148	0.85	2033	18.1	8.087
$(\text{Fe}_{0.5}\text{Co}_{0.5})_{90}(\text{Mo}_{0.1}\text{C}_{0.2}\text{B}_{0.5}\text{Si}_{0.2})_{10}$	63.5	3.1 ± 1.3	1.3 ± 1.1	2.8535	1355	1628	1523	0.97	2513	5.8	7.984
$(\text{Fe}_{0.5}\text{Co}_{0.5})_{85}(\text{Mo}_{0.1}\text{C}_{0.2}\text{B}_{0.5}\text{Si}_{0.2})_{15}$	49.3	2.2 ± 1.1	1.8 ± 1.3	2.8522	1338	1559	2020	1.33	2987	1.8	7.894
$(\text{Fe}_{0.5}\text{Co}_{0.5})_{80}(\text{Mo}_{0.1}\text{C}_{0.2}\text{B}_{0.5}\text{Si}_{0.2})_{20}$	86.8	4.7 ± 2.4	1.1 ± 0.9	2.8437	1298	1440	2690	1.39	2690	0	7.848
$(\text{Fe}_{0.5}\text{Co}_{0.5})_{70}(\text{Mo}_{0.1}\text{C}_{0.2}\text{B}_{0.5}\text{Si}_{0.2})_{30}$	—	—	—	2.8269	1283	1369	—	—	~550	—	7.700

*The properties listed are volume fraction of dendritic phase (f_d), average linear size of dendritic phase (l_d), lattice parameter of α -(Fe,Co) (a), melting temperature (T_m), liquidus temperature (T_l), yield strength (σ_y), yield strain (ε_y), compressive strength (σ_c), plastic strain (ε_p), and density (ρ).

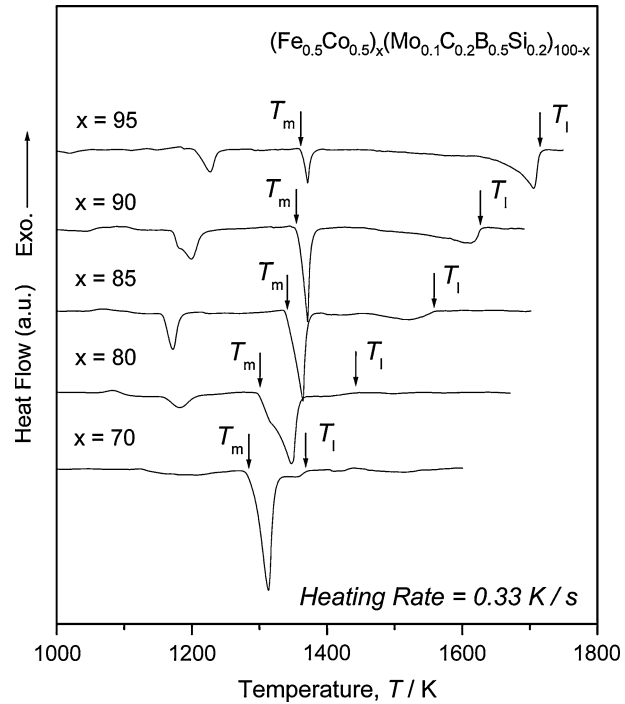


Fig. 2—DSC curves of $(\text{Fe}_{0.5}\text{Co}_{0.5})_x(\text{Mo}_{0.1}\text{C}_{0.2}\text{B}_{0.5}\text{Si}_{0.2})_{100-x}$ alloys ($x = 95, 90, 85, 80,$ and 70) at a heating rate of 0.33 K/s.

alloys are at the same hypoeutectic region. Combining with the information of the constituent phases for the three alloys, we can regard this FeCo-based multicomponent alloy system ($85 \leq x \leq 95$) as a simple (Fe,Co)-(Fe,Co)₃(B,C) pseudo-binary alloy system. This result makes it very convenient to analyze the following microstructural information in the corresponding alloys. As x is decreased further ($x = 80$ and 70), a new endothermic peak participates near T_m , which can be attributed to the appearance of the $(\text{Fe,Co})_{23}(\text{B,C})_6$ phase in the corresponding alloys. Although T_l keeps reducing gradually with decreasing x in these alloys, the solidus line of the former hypoeutectic region is destroyed. An endothermic peak near 1200 K can be observed in every sample, which corresponds to the phase transformation from α phase to γ phase.

The microstructure of these as-cast FeCo-based multicomponent alloys was observed by SEM (shown in Figure 3). The $(\text{Fe}_{0.5}\text{Co}_{0.5})_x(\text{Mo}_{0.1}\text{C}_{0.2}\text{B}_{0.5}\text{Si}_{0.2})_{100-x}$ alloys ($x = 95, 90,$ and 85) show a similar microstructure with tunable morphology and spatial distribution of constituent phases. Two kinds of composite structures can be found in different scales. One is in micrometer scale. The α -(Fe,Co) dendritic phase imbeds in the networklike eutectic phases consisting of α -(Fe,Co) and o -(Fe,Co)₃(B,C) phases to form a typical D-E composite structure (shown in Figures 3(a), (c), and (e)). The other is in nanometer scale. The ultrafine lamellar precipitate phase of $(\text{Fe,Co})_3(\text{B,C})$ homogeneously distributes in α -(Fe,Co) dendritic phase (shown in Figures 3(b), (d), and (f)). Both kinds of composite structures could influence the mechanical properties. As further increasing C and B concentration in the

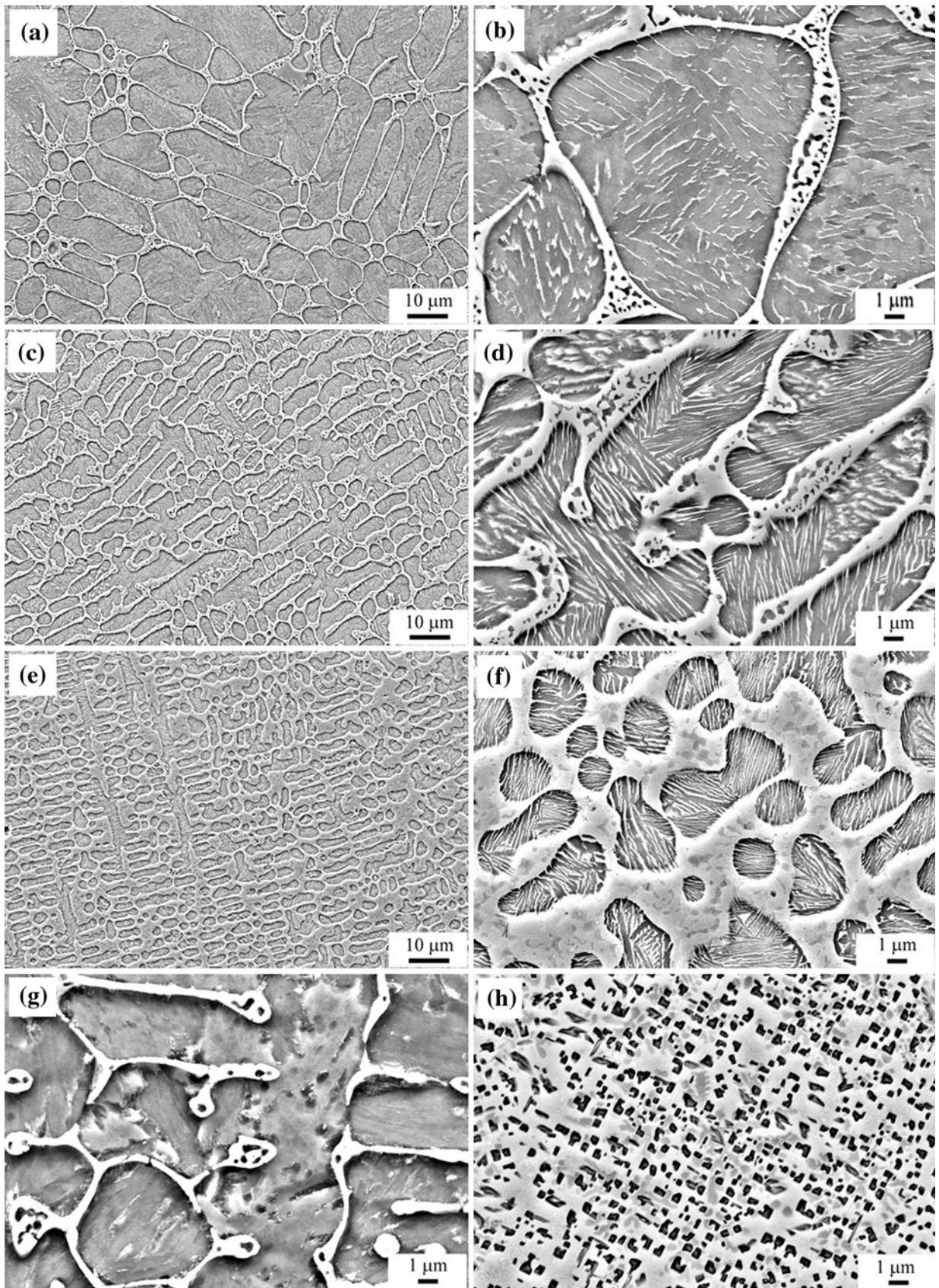


Fig. 3—Typical microstructure images of $(\text{Fe}_{0.5}\text{Co}_{0.5})_x(\text{Mo}_{0.1}\text{C}_{0.2}\text{B}_{0.5}\text{Si}_{0.2})_{100-x}$ alloys at different magnifications: (a) 1000 and (b) 4000 times for $x = 95$, (c) 1000 and (d) 4000 times for $x = 90$, (e) 1000 and (f) 4000 times for $x = 85$, (g) 4000 times for $x = 80$, and (h) 4000 times for $x = 70$.

FeCo-based alloys, the nanolamellar phase disappears in the specimen with $x = 80$. The coarse crystalline phase of $(\text{Fe,Co})_{23}(\text{B,C})_6$ can be observed in the dendritic phase, which might form through the solid reaction between $(\text{Fe,Co})_3(\text{B,C})$ and $\alpha\text{-(Fe,Co)}$ phases during solidification (shown in Figure 3(g)).^[19] The sample with $x = 70$ (shown in Figure 3(h)) exhibits a typical near-eutectic microstructure.

In order to obtain morphological characteristics of the FeCo-based multicomponent alloys, the method of quantitative microscopy was employed to identify the volume fraction and average linear size of the dendritic and eutectic phases,^[14] as listed in Table I. The value of the volume fraction of the dendritic phase (f_d) decreases from 79.8 to 49.3 pct with decreasing x from 95 to 85. The f_d (or the volume fraction of the eutectic phases $f_e = 1 - f_d$) is well linearly dependent on x , which indicates that the volume fraction of the constituent phases can be tunable by controlling the chemical composition of the multicomponent alloys in advance. For the sample with $x = 80$, the value of f_d is remarkably enlarged to 86.8 pct because the formation of $(\text{Fe,Co})_{23}(\text{B,C})_6$ phase induces the distribution of C and B elements in the constituent phases. The average linear sizes of the dendritic and eutectic phases (l_d and l_e) exhibit a similar change tendency of f_d and f_e .

Because the existence of brittle $(\text{Fe,Co})_{23}(\text{B,C})_6$ phase in the dendritic phase could seriously damage the plastic deformation ability of the as-cast samples with $x \leq 80$, we will only discuss the evolution of constituent phases and microstructure for the multicomponent alloys with $x = 95, 90,$ and 85 during the solidification process. Figure 4 shows schematically the temperature dependence of the constituent phases and morphology for these three alloys during solidification. As the temperature is above T_l , the alloy remains in the liquid state. The first solid phase precipitated from the melt is a high-temperature solid solution phase of (Fe,Co) dendritic cores with enrichment of Si, a certain amount of C, and little concentration of B. Because of the limited solid solubility of B in Fe/Co, the remaining melt will be continuously enriched in B to form a near-eutectic undercooled liquid.^[18] Although Mo and Si are substitutional solute elements to Fe and Co,^[18] only Si is completely dissolved in the primary (Fe,Co) solid solution because Mo shows a strong interaction with B.^[21] Therefore, the remaining melt will also be enriched in Mo. Considering of the ternary phase diagram of Fe-Si-C, the high-temperature phase of (Fe,Co) should be $(\delta\text{-Fe},\alpha\text{-Co})$ because the existence of Si will limit the formation of γ phase.^[19] This can give a reasonable explanation for the absence of γ phase in our system but the existence in other Fe-based multicomponent systems.^[9] With progressing solidification, the high-temperature (Fe,Co) dendritic phase grows bigger and bigger until solidification of the remaining undercooled liquid forms networklike eutectic phases. With further continuous cooling, the dendritic (Fe,Co) solid solution phase supersaturated in C and B is no longer stable. Finally, nanolamellar $(\text{Fe,Co})_3(\text{B,C})$ phase is precipitated in the dendritic phase, which could accompany the phase transformation from $(\delta\text{-Fe},\alpha\text{-Co})$ to $(\alpha\text{-Fe},\alpha\text{-Co})$.

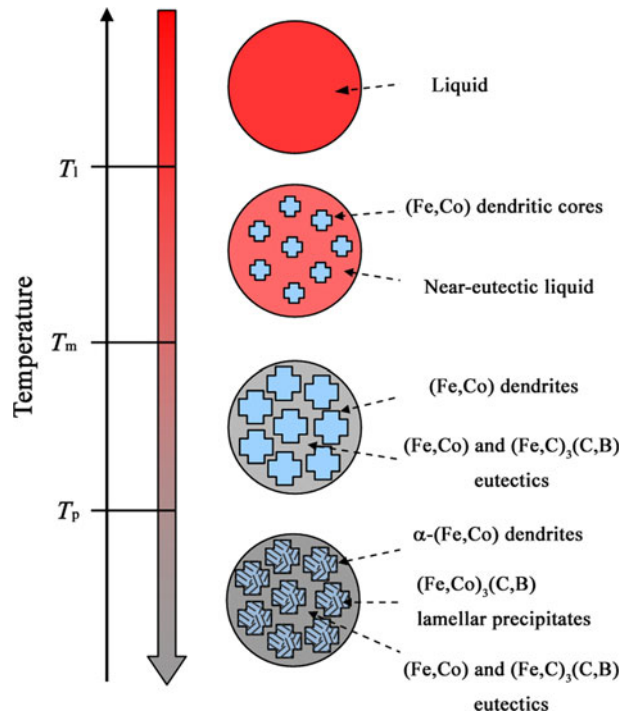


Fig. 4—A schematic illustration showing the evolution of constituent phases and microstructure for $(\text{Fe}_{0.5}\text{Co}_{0.5})_x(\text{Mo}_{0.1}\text{C}_{0.2}\text{B}_{0.5}\text{Si}_{0.2})_{100-x}$ alloys ($x = 95, 90,$ and 85) during the nonequilibrium solidification.

This expatiation could be helpful to understanding the formation and evolution of constituent phases in other D-E composites with similar composition and microstructure.

Table I also summarizes the mechanical behavior of the $(\text{Fe}_{0.5}\text{Co}_{0.5})_x(\text{Mo}_{0.1}\text{C}_{0.2}\text{B}_{0.5}\text{Si}_{0.2})_{100-x}$ alloy ($x = 95, 90, 85, 80,$ and 70). There one can observe that the yield strength and the yield strain increase as the metalloid content increases, *i.e.*, atomic fraction x decreases. Due to the changes in morphology, the samples become tougher and the fracture strength increases, but the plastic deformation decreases, from 18.1 pct in the case of $(\text{Fe}_{0.5}\text{Co}_{0.5})_{95}(\text{Mo}_{0.1}\text{C}_{0.2}\text{B}_{0.5}\text{Si}_{0.2})_5$ to almost 0 for $x < 80$ pct. The embrittlement can be attributed to the presence of a higher percentage of C, B, and Si.

IV. CONCLUSIONS

A family of $(\text{Fe}_{0.5}\text{Co}_{0.5})_x(\text{Mo}_{0.1}\text{C}_{0.2}\text{B}_{0.5}\text{Si}_{0.2})_{100-x}$ multicomponent alloys ($x = 95, 90, 85, 80,$ and 70) were produced by copper mold casting. Two kinds of metastable (Fe,Co)-(B,C) phases were found in as-cast samples. One is Fe_3C -type $o\text{-(Fe,Co)}_3(\text{B,C})$ phase existing in all samples; and the other is Cr_{23}C_6 -type $(\text{Fe,Co})_{23}(\text{B,C})_6$ phase, which can be found in the x range from 80 to 70. Morphological characteristics of dendritic and eutectic phases were identified by quantitative microscopy, which indicated that the volume fraction of constituent phases can be tunable by adjusting the chemical compositions in partial composition range ($85 \leq x \leq 95$). The evolution of constituent

phases and microstructure for the multicomponent alloys in this composition range was illustrated, which could be applicable to understanding the morphologic formation of these D-E composites.

ACKNOWLEDGMENTS

The authors thank Dr. H. Wendrock for his valuable help with the SEM image analysis. One of the authors (RL) acknowledges the fellowship support from the Alexander von Humboldt Foundation.

REFERENCES

1. A. Inoue: *Acta Mater.*, 2000, vol. 48, pp. 279–306.
2. W.L. Johnson: *Mater. Sci. Forum*, 1996, vol. 225, pp. 35–49.
3. W.H. Wang, C. Dong, and C.H. Shek: *Mater. Sci. Eng. R*, 2004, vol. 44, pp. 45–89.
4. M.F. Ashby and A.L. Greer: *Scripta Mater.*, 2006, vol. 54, pp. 321–26.
5. G. He, J. Eckert, W. Loser, and L. Schultz: *Nat. Mater.*, 2003, vol. 2, pp. 33–37.
6. J. Eckert, G. He, J. Das, and W. Loser: *Mater. Trans.*, 2003, vol. 44, pp. 1999–2006.
7. U. Kuhn, N. Mattern, T. Gemming, U. Siegel, K. Werniewicz, and J. Eckert: *Appl. Phys. Lett.*, 2007, vol. 90, p. 261901.
8. J.M. Park, S.W. Sohn, D.H. Kim, K.B. Kim, W.T. Kim, and J. Eckert: *Appl. Phys. Lett.*, 2008, vol. 92, p. 091910.
9. K. Werniewicz, U. Kuhn, N. Mattern, B. Bartusch, J. Eckert, J. Das, L. Schultz, and T. Kulik: *Acta Mater.*, 2007, vol. 55, pp. 3513–20.
10. A.R. Yavari, K. Ota, K. Georgarakis, A. LeMoulec, F. Charlot, G. Vaughan, A.L. Greer, and A. Inoue: *Acta Mater.*, 2008, vol. 56, pp. 1830–39.
11. L.L. Shi, H. Ma, and T. Liu: *J. Mater. Res.*, 2006, vol. 21, pp. 613–22.
12. Y. Li, K. Georgarakis, S.J. Pang, J. Antonowicz, F. Charlot, A. LeMoulec, T. Zhang, and A.R. Yavari: *J. Alloys Compd.*, 2009, vol. 477, pp. 346–49.
13. R. Li, G. Liu, M. Stoica, and J. Eckert: *Intermetallics*, doi: [10.1016/j.intermet.2009.07.003](https://doi.org/10.1016/j.intermet.2009.07.003).
14. R.T. DeHoff and F.N. Rhines: *Quantitative Microscopy*, McGraw-Hill, New York, NY, 1968.
15. J.A. Dean: *Lange's Handbook of Chemistry*, 15th ed., McGraw-Hill, New York, NY, 1998.
16. Y. Khan, E. Kneller, and M. Sostarich: *Z. Metallkd.*, 1982, vol. 73, pp. 624–26.
17. P. Villars and L.D. Calvert: *Pearson's Handbook of Crystallographic Data for Intermetallic Phases*, 2nd ed., ASM INTERNATIONAL, Materials Park, OH, 1991.
18. T.B. Massalski, H. Okamoto, R.P. Subramanian, and L. Kacprzak: *Binary Alloy Phase Diagrams*, 2nd ed., ASM INTERNATIONAL, Materials Park, OH, 1991.
19. V. Raghavan: *Phase Diagrams of Ternary Iron Alloys*, Indian Institute of Metals, Calcutta, 1992.
20. M.L. Borlera and G. Pradelli: *Metallurgia Italiana*, 1967, vol. 59, pp. 907–16.
21. F.R. de Boer, R. Boom, W.C.M. Mattens, A.R. Miedema, and A.K. Niessen: *Cohesion in Metals*, North-Holland, Amsterdam, The Netherlands, 1989.